Muon detection as geophysical prospecting method: a barite ore modeling

F. Coren[1], E. Caffau[2] and S. Spagnul[3]

[1] *Istituto Nazionale di Oceanografia e di Geofisica Sperimentale, Trieste, Italy*
[2] *Convitto Nazionale Paolo Diacono, Cividale del Friuli, Italy*
[3] *Via Marchesi 3, Aquileia, Italy*

Abstract - In 1995 a joint INFN – OGS experiment named μGA successfully applied the muon detection method to geophysical prospecting. Taking into account the results of this experiment, we model the possible applications and limits of this method in a real case constituted by a schematic barite ore deposit embedded in a sandstone matrix. A muon detector similar to that used in the 1995 experiment was simulated at the bottom of the ore (100 m depth) and the received muon flux modeled. The expected muon flux was spread according to a Poisson distribution in order to simulate a real measurement. The simulated acquisition provided the input data for the solution of the inverse problem. The target of the modelling was to reconstruct the density distribution of the rock volume as seen by the muon detector in its surroundings. This enables us to outline capabilities and limits of such a method in imaging the barite ore and at the same time its geophysical prospecting potential. Modelling results indicate that the method can be positively addressed to a real case.

1. Introduction

The shower of cosmic rays that continuously impinges the Earth's surface presents a wide spectrum of energy; among all the types of particles associated with this event, muons are the most penetrating ones. The muon flux penetrates the Earth's surface and is reduced proportionally to the quantity of mass crossed. Underground measurement of the muon flux provides, therefore, excellent information on the mass that muons penetrate, starting from the instant in which they meet the Earth's surface, up to the moment they are detected. The use of

Corresponding author: F. Coren, Ist. Naz. Oceanografia e Geofisica Sperimentale, Borgo Grotta Gigante 42c, 34010 Sgonico (Trieste), Italy; phone: +39 0402140255; fax +39 040327307; e-mail: fcoren@ogs.trieste.it

underground muon flux measurement in geophysics has already been outlined by a previous experiment conducted by some of the authors in 1995. The joint INFN (Istituto Nazionale di Fisica Nucleare) – OGS (Istituto Nazionale di Oceanografia e di Geofisica Sperimentale) experiment named μGA, successfully demonstrated the application of the muon detection method in the morphological reconstruction of an underground cavity (Caffau et al., 1996). Taking into account the results of the μGA experiment, we investigate in this paper the possible exploitation of this methodology in mining geophysics by modelling a muon flux crossing a barite ore deposit of cylindrical shape, included in a sandstone matrix. This is a really simple geometrical assumption for an ore but nevertheless accurate enough to investigate the method's capabilities and limits. A muon detector has been simulated at the bottom of the ore (100 m depth) and the muon flux modelled. The simulated acquisition provided the input data for the solution of the inverse problem. A Poisson error distribution has been applied in order to simulate the error distribution of a real measurement. The modelled data were then inverted to achieve an image of the underground mass distribution simulating the real acquisition run. This enables us to demonstrate the applicability of such a method in the field of geophysical prospecting and, at the same time, to image the barite ore.

2. The muon tracking apparatus

We simulated the muon tracking apparatus (MTA) deriving the characteristics from the real device used in 1995 during the μGA experiment. The MTA is composed of four parallel scintillating planes constituted by series of glass chambers filled with a mix of argon-isobutane-freon gas (Caffau et al., 1996). A charged particle, crossing the gas contained in every single chamber, ionizes the gas and determines a local discharge detectable as an electric signal. By reconstructing the track of the signal along the detector planes, it is possible to compute direction (zenit (θ) and azimuth (φ) angles) for every single event. The number of events is related to the detector surface, to the acquisition time and depends inversely on the quantity of mass crossed by muons. The MTA we modeled is made of four counter planes, placed on top of each other at a distance of 0.20 m. Each plane has a surface of 1 m^2 (Fig. 1) and is constituted by an orthogonal grid of 100 plastic scintillator rods. Every rod has a surface of $0.02 \cdot 1.00$ m^2; for each plane an efficiency of about 0.9 has been assumed. From the energy released by the particles, at different position in each of the four planes (or al least three of them), the direction of each incoming muon is reconstructed. Because of the granularity of the detector, the resolution depends on the zenith θ, and azimuth φ, angles of the incoming muons. The resolution in the two angular directions θ and φ (on the XZ and YZ planes) have the following expressions:

$$\delta\theta = \left(\arctan \frac{s}{l}\right) \cdot \left(\frac{1}{1 + \tan^2 \theta}\right) \tag{1}$$

$$\delta\phi = \left(\arctan \frac{s}{l}\right) \cdot \left(\frac{1}{\tan \theta}\right) \tag{2}$$
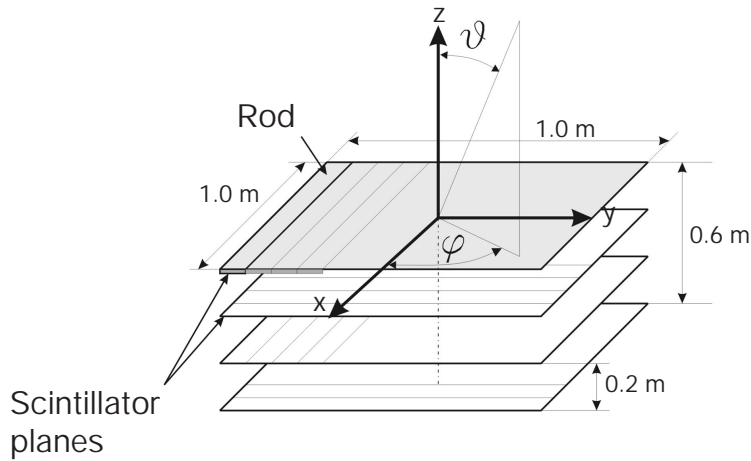
Fig. 1 - Detector scheme. Four 1 m^2 counter planes are placed on top of each other. Each plane is formed by 100 plastic scintillator rods (each with surface 0.2 · 1 m^2). On each plane, the rods are placed in two layers, orthogonal to each other, in such a way as to create a Cartesian reference system.

where l is the distance between the top and the bottom planes, and s is the width of each rod. The two functions, for $l = 0.60$ m and $s = 0.02$ m, are shown in Figs. 2 and 3. The zenith resolution is a decreasing function, always smaller than 2°; the azimuth resolution is a function of θ and diverges for $\theta \rightarrow 0$; however for $\theta > 20°$ $\delta\varphi < 5°$. Therefore, we considered solid angle bins of acceptance with a dimension of $\Delta\Omega\theta = \sin\theta \cdot \Delta\Omega \cdot \Delta\varphi = \sin\theta \cdot 2° \cdot 5°$. With this bin size, the resolution in θ is always smaller than the bin size, and the resolution in φ is comparable or smaller than the bin size itself, at least for $\theta > 20°$. The bin dimension controls not only the resolution but also the acquisition time. This, because in order to have robust statistics we need
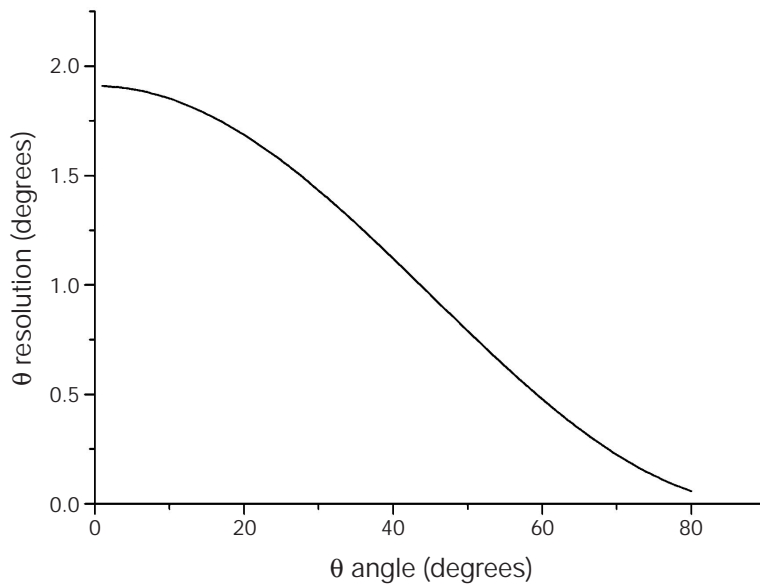
Fig. 2 - Zenith resolution function of the detector. This is a decreasing function of θ. Muons impinging on the detector with small θ angle have the greatest resolution, but anyway smaller than 2°.
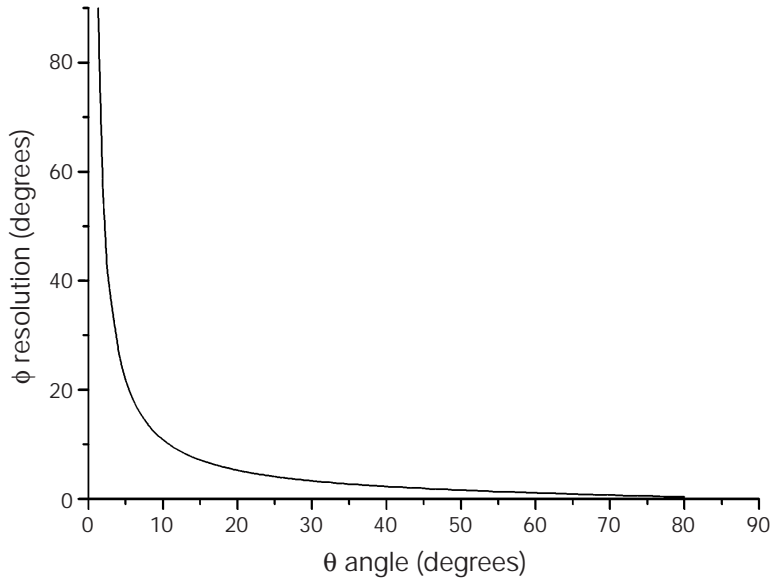
Fig. 3 - Azimuth resolution function of the detector. This is a decreasing function of θ. This function is not defined for $\theta = 0$ and diverges as θ approaches zero.

to count a sufficient number of events in each bin. Practically, to maintain the acquisition statistics at a reliable level without considering exaggerated acquisition time (order of months) we have to find a compromise in setting all these variables. The acceptance of the detector is function of the direction of the incoming muon flux (zenith and azimuth angle), the average efficiency of the detector, and, the distance between the planes of the detector as described by the following expressions:

$$A\,(\Theta,\,\phi,\,\varepsilon,\,l) = \left[2\left(l - \frac{l}{3}\tan\theta\cos\phi\right)\cos\theta\left(l - \frac{l}{3}\tan\theta\sin\phi\right)\right]\varepsilon 2 +$$

$$+\left[2\left(l - \frac{2l}{l}\tan\theta\cos\phi\right)\cos\phi\left(l - \frac{2l}{3}\tan\theta\sin\phi\right)\right]\frac{\varepsilon^3}{2 - 3\varepsilon}\cdot \tag{3}$$

3. Muon flux expectation

The muon differential flux underground can be theoretically evaluated using the following distribution function (Gaisser, 1990) as:

$$\frac{d^2\,N_\mu}{d\Omega dt} = \int_{E_0^{min}}^{E_0^{max}} \frac{d^3\,N_0}{dE_0\Omega dt}\,dE_0, \tag{4}$$

E_0^{max} is the maximum muon energy, theoretically infinity, that we set at 1000 TeV in the simulation. E_0^{min} is the minimum energy that a muon must have to reach the detector crossing the

lithosphere. E_0^{min} is function of the linear density lr crossed by the muon which is function of the depth crossed by the muon s, and of the density of the layer crossed ρ: $lr = s \cdot \rho$, (so that $[lr]$ = gcm^{-2}). The minimum energy in every direction depends on the morphology of the area above the detector site and on the density distribution of the crossed material:

$$E_0^{min} = \varepsilon \left(\varepsilon^{\chi/\xi} - 1 \right) \tag{5}$$

$\varepsilon = \alpha \cdot \xi$ is the critical energy, which is particle - and medium - dependent, for muons in rock $\varepsilon \approx 500$ GeV (Gaisser, 1990); when the muon energy is greater than ε, discrete processes (pair production, bremsstrahlung, nuclear interaction) are dominant, on the contrary, when the muon energy is smaller than ε continuum processes (ionization, Cerenkov) are dominant:

$\xi = (\xi_{\text{bremstrallung}}^{-1} + \xi_{\text{pair}}^{-1} + + \xi_{\text{hadronic}}^{-1})^{-1} \approx 2.5 \ 10^{-1}$ gm^{-2} in rocks (Gaisser, 1990).

We derived the value of the mass crossed by muons as a function of the azimuth angle, φ, and the zenith angle, θ, from a model of the mine of barite. For the muon differential intensity, dN_μ/dE_μ in Eq. (4) (Dar, 1983) suggests:

$$\frac{d^2 N_\mu}{dE_\mu} \propto \Sigma_M \ gM^{at} \ BM \ \alpha \ MS_\mu \ (\bar{E}) \ [Km \ (E_0) - KM \ (\beta \ ME_0)], \tag{6}$$

which is in good agreement with experimental data for values of linear density relevant to our simulation. The meaning of the symbols in Eq. (6) can been found in Tables 1 and 2. The integral in Eq. (4) may be computed numerically and the muon flux under a rock layer measured for our detector site can be computed as follows:

$$\frac{d^2 N_\mu}{d\Omega dt} = \left[\int_{E_0^{min}}^{E_0^{max}} \frac{d^3 N_0}{dE_0 \ d\Omega dt} \ dE_0 \right] A \ (\Omega, \ \varepsilon), \tag{7}$$

where $A(\Omega, \varepsilon)$ is the acceptance Eq. (3) and ε is the efficiency of the detector. So the theoretical muon flux value in each solid angle element $A\Omega \ (\theta_i, \ \varphi_i)$ is:

Table 1 - Useful formulas.

$S\mu \ (\bar{E}) = \left(\dfrac{\lambda_0}{\lambda_F} \right)^{\frac{1}{\gamma_\mu \bar{E}}}$	probability μ reaches sea level before decay
$\bar{E} = E + \dfrac{\alpha}{2} \ (\lambda_F - \lambda_0)$	average energy in atmosphere
$E_0 = E + \alpha \ (\lambda_F - \lambda_0)$	approximate born energy for muons at zenith angle
$\gamma_\mu = \dfrac{\tau_\mu \cos\theta}{m_\mu \ c \ h_0}$	
$K_M \ (E) \propto \dfrac{E^{-p}}{p + (p + 1) \ \gamma_M \ E}$	
$\gamma_M = \dfrac{\tau_M \cos\theta}{m_M \ c \ h_0}$	
$M = \pi$ pion component	$M = K$ kaon component

Table 2 - Physical quantities

λ_0	120g	
λ_F	$\dfrac{1030}{\cos\theta}$ gcm^{-2}	atmospheric depth
B_π	1	branching ratio in pion
B_k	0.635	branching ratio in kaon
α_π	2.34	$\dfrac{m_\pi^2}{(m_\pi^2 - m_\mu^2)}$
α_k	1.05	$\dfrac{m_k^2}{(m_k^2 - m_\mu^2)}$
β_π	1.74	$\dfrac{m_k^2}{m_\mu^2}$
β_k	21.7	$\dfrac{m_\pi^2}{m_\mu^2}$
α	2.06 MeV cm^2/g	energy losses $\rho^{-1}\frac{dE}{dx}$
h_0	6.3 km	scale parameter of the upper atmosphere
m_μ	106 $\dfrac{\text{MeV}}{c^2}$	muon mass
τ_μ	2.2×10^{-6}s	muon life time
m_τ	140 $\dfrac{\text{MeV}}{c^2}$	pion mass
τ_π	2.6×10^{-8}s	pion life time
m_k	494 $\dfrac{\text{MeV}}{c^2}$	kaon mass
τ_k	1.24×10^{-8}s	kaon life time
g_M^{at}	$\Lambda_\pi = 160$ gcm^{-2}	attenuation for pion
g_M^{at}	$\Lambda_K = 180$ gcm^{-2}	attenuation for kaon

$$N_\mu(\theta_i, \varphi_j) = \Delta t \Delta\Omega(\theta_i, \varphi_j) A(\Omega(\theta_i, \varphi_j), \varepsilon) \left[\int_{E_0^{min}}^{E_0^{max}} \frac{d^3 N_0}{dE_0 \, d\Omega dt} dE_0 \right] \qquad (8)$$

with Δt (s) is the measurement time, $i = 1,....35$ (θ bin width is 2°), $j = 1,...,72$ (φ bin width is 5°). We simulate the detection of muons with a zenith angle not greater than 70°.

4. Geological model

We designed the mine model as a simple ore, constituted by a cylindrical deposit (see Fig. 4). Even though the shape of the ore is a really simple one, it mimics barite bodies as those located in Ballynoe at Silvermines (Ireland) (Larter et al., 1981), or at Meggen and Rammelsberg (Germany) mines (Clark et al., 1990). The barite deposit density we adopted is 3200 kg·m^{-3} and the ore is inserted within a limestone clastic deposit for which we adopted a density of 2700 kg·m^{-3}. We assumed that our ore model is a satellite deposit of a mine which shafts and levels allows to install a muon detector at the depth of 100 meters underground and in direct sight of

the deposits (see Fig. 4). We simulated an acquisition run of the detector, 60 days long. From an economical point of view, we need to highlight that the acquisition procedure is an automatic process which requires only the power supply of the device and very reduced manned controls.

5. Muon simulation run

Keeping in mind that the method is sensitive to the variation in the mass crossed by the muons to reach the detector, we compared the theoretical expected muon flux in cases where the baryte ore is or is not present. Fig. 5 shows the expected muon flux with and without the barite as a function of the azimuth angle, φ, for several bins in the zenith angle, $20° < \theta < 40°$. As can be seen, there is a disagreement in the two muon flux distributions caused by the presence of the barite that reduces the number of detectable events. In fact, muons impinging on the detector with an azimuth angle in the range of $87.5° < \varphi < 92.5°$, cross the barite ore, and this implies that the linear density up to the detector is, for equal depth, greater than in case when muons do not cross the barite. The comparison of muon flux as function of zenith angles, θ, has no interest, because for few values of φ ($87.5° < \varphi < 92.5°$) the detected muons actually cross the barite, whereas for most values of φ they do not, so that the difference is not appreciable. In fact, the difference in linear density with or without the barite ore is very small and affects each θ bin in more or less the same way. We adopted a Poisson noise to model a real acquisition. The
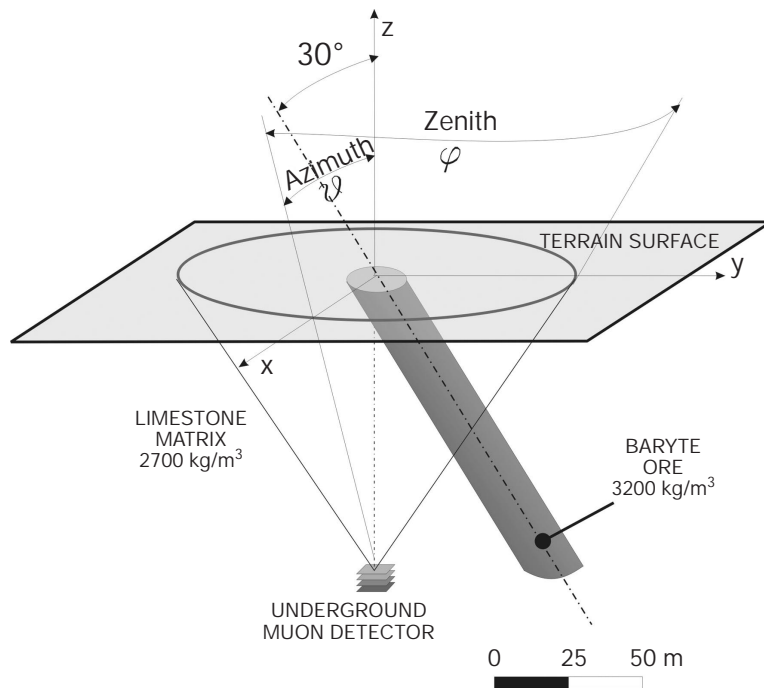
Fig. 4 - Sketch of the test site. The detector is located below the rectangle that indicates the terrain surface. The cone shows the region from which muons impinging on the scintillator are detected. The inclined grey cylinder represents the barite one.
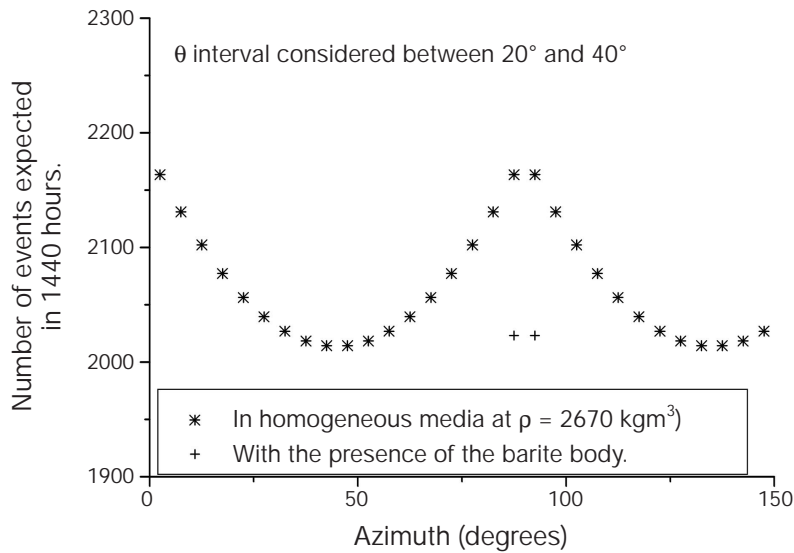
Fig. 5 - Muon flux versus azimuth for 20° < theta < 40°. Stars represent the muon flux at the selected theta as a function of azimuth angle without the barite one. The crosses represent the same muon flux in presence of the barite ore. Only in correspondence to the azimuth angle along the direct sight of the barite ore are the two fluxes different.

noise was added to the flux, as given by Eq. (7). Fig. 6 shows the normalised difference between the expected muon fluxes with and without the barite ore. The difference is reported bin by bin, versus the horizontal distance from the detector, using a polar stereographic projection centered on the detector. The signature of the barite can be seen in the plot as a triangle-shaped anomaly. The great difference with a circular distribution, in the vicinity of the detector zenith, is an artifact due to the coarse resolution in azimuth for angles near the vertical of the detector. We compute the expected barite thickness plotted versus the horizontal distance from the detector, without taking into account the Poisson error as shown in Fig. 7. The thickness has been computed using the difference between the expected linear density with and without the barite cylinder. The difference has then been divided by 3.2 which represents the density of the barite. The plot clearly shows the barite distribution and thickness. Fig. 8 shows the barite thickness, as reconstructed by the muon detector, considering the Poisson error. The thickness has been computed by subtraction of the reconstructed linear density, as derived from simulated measured flux (Poisson error), with barite and the linear density without the barite. This plot represents the barite signature as seen by the detector after an acquisition run of 60 days. Discrepancies between this result and the "theoretical" one, as shown in Fig. 7, is mainly due to the azimuth resolution and the Poisson error which affects a real measurement. The shape of the barite cylinder can be spotted and its thickness can be outlined with a resolution higher than 2 meters. The reconstructed barite thickness shape suffers from a strong distortion because of the projection adopted. We suppose that a more accurate density distribution reconstruction can be achieved using tomographic techniques. All the acquisition runs we simulated were in the last 60 days (1440 hours). This time represents a good compromise between operative timing and resolution.
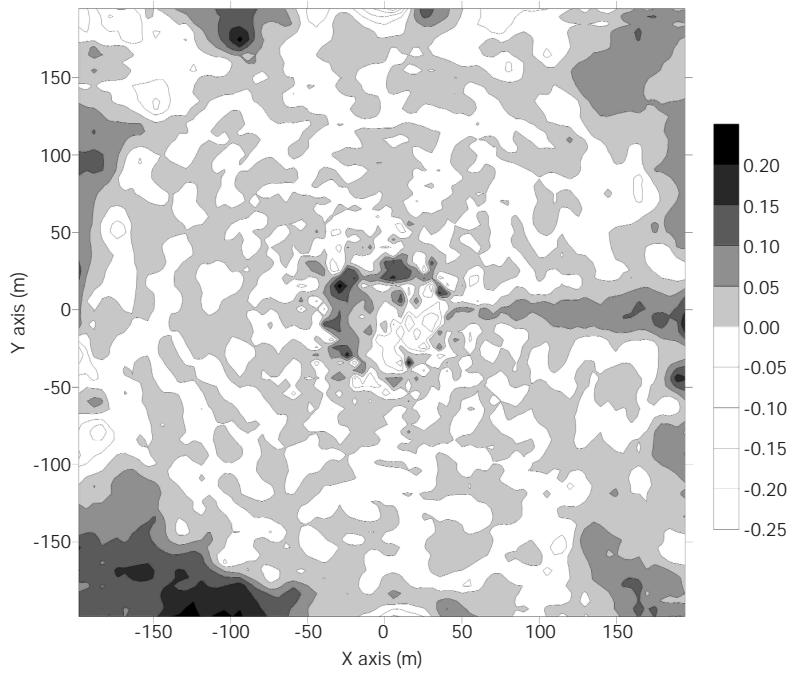
Fig. 6 - Normalized difference between simulated muon fluxes with baryte and without baryte. The presence of the baryte can be identified by the large triangular shaped anomaly located along the positive X semi-axis. The area located at the proximity of the axis origin, the detector vertical, is strongly affected by the coarse θ resolution function.
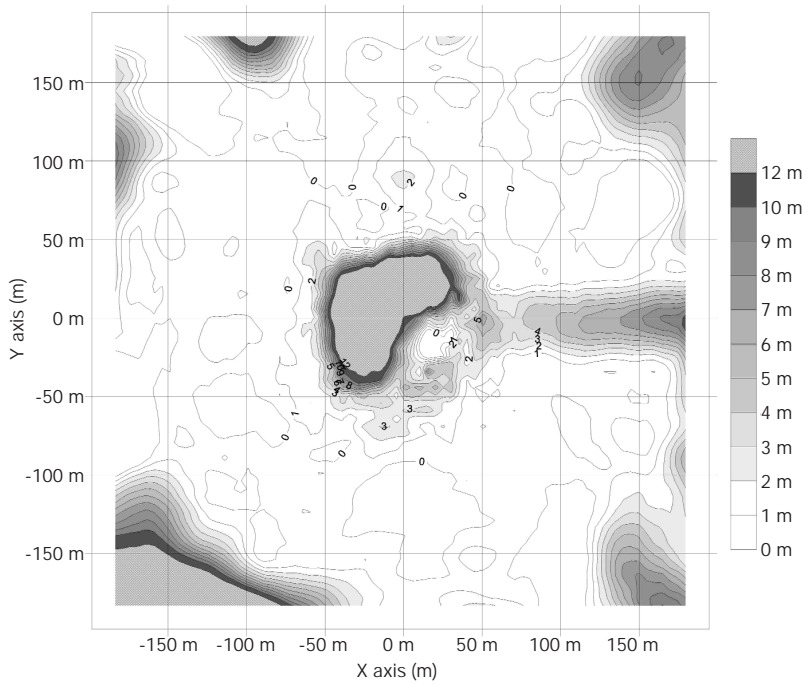
Fig. 7 - Expected baryte thickness versus the horizontal distance from the detector computed taking into account the Poisson error function. The plot shows the barite distribution and thickness.
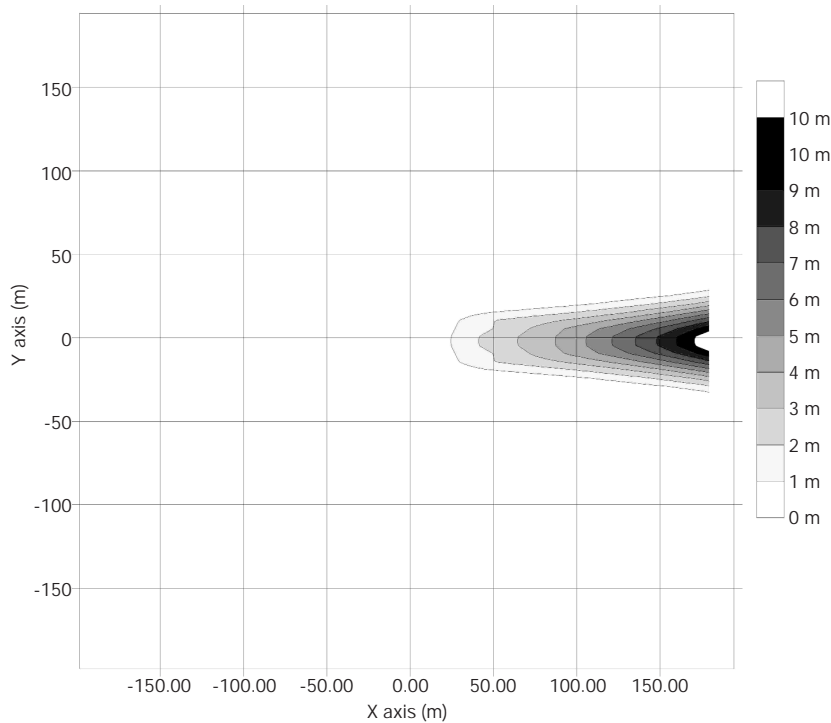
Fig. 8 - Baryte thickness as reconstructed by the muon detector after removal of artifacts and after application of a spatial filtering. The shape of the baryte cylinder can be outlined with an resolution higher than 2 meters.

6. Discussion

The choice of the acquisition time is a compromise between obtaining a large statistic, so that the signal to noise ratio allows an unambiguous detection of a barite ore, and keeping the operating costs low. The cost of operating the detector is mainly due to the immobilization of the device and the power supply; with this concept in view, an acquisition time as long as several weeks is feasible. The choice of the binning and, consequently, the resolution, is related to the acquisition time. We fixed it as $\Delta\Omega\theta = \sin\theta \cdot 2° \cdot 5°$ in this way we fully exploit the detector resolution. Greater $\Delta\Omega$ means smaller acquisition time, but also smaller resolution. Smaller $\Delta\Omega$ means over sampling and is not convenient in this context. Using a larger detector, the acquisition time can be smaller to obtain the same statistic. The optimal range of operation of the detector is $20° < \theta < 50°$. For a smaller θ the resolution in φ is quite large ($\Delta\varphi > 5°$), so that we cannot distinguish between directions which are too close; for a greater θ the muon flux is reduced and, consequently, the statistics. These considerations suggest a possible strategy of acquisition. Starting with an acquisition for a relatively short time and then, if an anomaly is found in the range of $20° < \theta < 50°$, continue with the acquisition in order to improve statistics. If the anomaly is located outside this range in θ, it is preferable either to move the detector in such a way that the anomaly falls in the range $20° < \theta < 50°$ or, if the anomaly is for $\theta > 50°$, differentially displace the single planes of the detector to improve the geometrical acceptance (effective area) in that direction.

7. Conclusions

The results of the simulation described in this paper, indicate that muon detection can represent an innovative and realistic geophysical prospecting method for underground density imaging. The results of this modeling indicate that even though some aspects of the acquisition system still have to be improved, especially in the detector resolution and dimension, at the present state-of-the-art a "field" application could be feasible. The method can be used to identify targets characterised by relatively high density contrast with respect to the matrix, as massive ore bodies or cavities. The location of the targets is constrained by the possibility of locating the detector beneath the target and in its direct sight. This geometrical limit can be worked around using "bore hole designed detectors" for which a development technology already exists.

References

Dar A.; 1983: *Atmospheric Neutrinos, Astrophysical Neutrons, and Proton--Decay Experiments.* Physical Review Letters pp 5, 227.

Caffau E., Coren F. and Giannini G.; 1996: *Underground cosmic-ray measurement for morphological reconstruction of the "Grotta Gigante" natural cave.* Nuclear Instruments & Methods in Physics Research **A385**, 480-488.

Clark S.H.B., Gallagher M.J. and Poole F.G.; 1990: *World baryte resources: a review of recent production patterns and genetic classification.* Trans. Instn. Min. Metall. (Sec. B Appl. Earth Sci.), **99**, B125-32.

Gaisser T.K.; 1990: *Cosmic Rays and Particle Physics.* Cambridge University Press, Cambridge (UK), pp. 76-79.

Larter R.C.L., Boyce A.J. and Russell M.J.; 1981: *Hydrothermal pyrite chimneys from the Ballynoe baryte deposit, Silvermines, Country Tipperary, Ireland.* Mineral Deposita **16**, 487-96.